DOI 10.24425/aee.2023.145413

Stator current spectrum analysis of a double cage induction motor with rotor asymmetry

JAROSŁAW TULICKI ✉, TADEUSZ JAN SOBCZYK, MACIEJ SUŁOWICZ

Department of Electrical Engineering
Faculty of Electrical and Computer Engineering
Cracow University of Technology
24 Warszawska str., 31-155 Kraków, Poland
e-mail: {✉jtulicki/tsobczyk/msulowicz}@pk.edu.pl

(Received: 20.06.2022, revised: 08.11.2022)

Abstract: This study presents a method to directly calculate the stator current Fourier spectra in double-cage induction motors to diagnose faults in rotor cages. A circuit model is developed for this purpose, allowing the modelling of any asymmetry in the outer and inner rotor cages. The model extends the conventional model of a cage motor by considering the higher space harmonics generated by the stator windings. The asymmetry of the cages is modelled by growing the resistance of any of the rotor bars. This results in various model equations, to be solved by looking for diagnostic signals. Motor current signature analysis is typically used to diagnose cage motors based on the Fourier spectra of the stator currents during steady-state operation. This study determines these spectra for double cage motors using the harmonic balance method, omitting the transient calculations. The calculation results confirmed the sensitivity of the stator current Fourier spectra as a diagnostic signal to distinguish faults in the outer and inner cages.

Key words: cage asymmetry, double cage induction motor, harmonic balance method, steady-state analysis, stator current Fourier spectra

1. Introduction

Double cage induction motors are commonly used medium and high-powered AC machines. The specific rotor design requires a relatively high number of individual elements that should be distinguished considering the cage asymmetry: $2N$ rotor bars for a rotor with N slots, $2N$ end-ring segments if the end-rings of each cage are separate, or N end-ring segments for a cage

with common end-rings, found in medium powered motors up to 100 kW [12,19]. A high number of cage elements significantly complicates the diagnosis of a double cage rotor compared with one-cage rotors.

Double cage rotors are particularly vulnerable to electrical damage owing to their transient thermal phenomena. Damage typically occurs during long term transients, caused by a large moment of inertia of a drive or level of load [11, 23]. During such operations, the starting cage is mostly loaded and often damaged. Damage to the working cage occurs much less frequently, primarily because of overloading at steady states. Despite this, diagnosing a double cage rotor requires distinguishing between faults in the starting (outer) and working (inner) cages.

The electrical asymmetry in a double cage rotor is similar to those in a one-cage rotor. As the temperature of the stator winding increases, the efficiency and maximal and starting torques decrease. Uneven distributions of currents in rotor cages negatively affect the mechanical system, increasing vibration and excessive load on the bearings caused by increased magnetic tension forces. The level of negative phenomena depends on the location of the damaged bars in the cage. Damage to a few neighbouring bars in the starting cage can substantially impedes the starting procedure and force current flow through the rotor yoke to destroy the sheet packets. The distribution of broken bars in the cages determines the level of stator current fluctuation in steady states and generates an alternating component of the electromagnetic torque. For double-cage motors, transient processes are determined by the outer cage; however, steady states at small slips depend primarily on the inner cage. These essential features were applied in diagnosing a double cage rotor. Diagnostic signals for the outer cage are based on signals at transients using time-frequency methods. By contrast, signals for the inner cage are based on the frequency spectra of stator currents in steady states at sufficiently high loads. Applications of the above-mentioned phenomena for diagnostic purposes are presented in various studies on one cage and double cage motors.

Limited studies on the asymmetry of double cage induction motors can be found in the literature. Most studies present the measurement results for experimental test stands with rotors specially prepared to damage the bars in the outer and inner cages [13, 16, 17, 24]. Electrical and mechanical quantities were measured and analysed for transient start up [15–17] and steady-states operations [18, 24, 25, 28]. These results allow us to recognise the effects of cage damages and suggest algorithms for rotor diagnostics. Stator currents, often used for diagnostics, are characterised using the time-frequency method for transients [15, 21, 22]. By contrast, methods based on frequency and statistical analysis are applied for steady states [5, 24, 25]. Studies used to analyse mathematical models of double cage motors under faulty conditions prefer field models [7, 26, 27], however, circuital models are also present [5]. The analyses focus on stator current properties using various measures; strategies for diagnostics are proposed according to the results.

This study presents an approach to predict the Fourier spectra of stator currents for a double cage motor at arbitrary damage to bars in the outer and inner cages. The mathematical model of these motors is presented as ordinary differential equations for all circuits on the stator and rotor sides by extending a known circuit model of typical cage motors, considering the higher space harmonics generated by the stator and rotor windings [1, 4, 6, 8, 14, 20]. The double cage on the rotor increases the number of rotor equations by twice in this model; thus, the number of model equations to be solved for diagnostic signals is rather high.

Detailed assumptions for the model are provided in the respective chapters. The parameters for this model can be calculated using "classical" formulas for inductances and resistances in AC machines based on geometrical and materials data [9, 12, 19]. The asymmetry of the cage is modelled by increasing the resistance of any of the $2N$ rotor bars.

Motor current signature analysis (MCSA) is typically used in diagnosing cage motors based on the Fourier spectra of stator currents during steady-state operations. In this study, these spectra were directly obtained using the harmonic balance method for the differential equation set constituting the mathematical model of double cage motors. To evaluate the sensitivity of this approach, the following calculations were performed. The Fourier spectra of stator currents were calculated for steady states at near rated loads if faults in the outer or inner cage appear separately and if the faults occur both in the outer and inner cages. These tests indicate faults in the inner cage. Faults in the outer cage can be observed in the stator currents during the transients. The outer cage can also be activated, generating an opposite rotating magnetic field in the motor. Furthermore, the effects of the outer cage asymmetry should be observed in the Fourier spectra of the stator currents at the steady state. This allows omitting the simulations of transients, which are time consuming owing to the high number of mathematical model equations. Subsequently, Fourier spectra should be calculated by repeating the abovementioned tests on the unloaded motor and growing the resistance of one from the stator phases to simulate a one-phase break and indicate faults in the outer cage.

2. Circuital model of double cage induction motors

The mathematical model of the double-cage motors presented below is designed to study asymmetry in rotor cages; both the magnetic circuit and stator windings are assumed to be symmetrical. Therefore, the three-phase stator winding generates magneto-motive forces with odd harmonics of orders p, $3p$, $5p$, $7p$, (p – pole-pair number), located symmetrically on the circumference. Moreover, the rotor has N slots, in which the bars of the outer and inner cages are laid and connected by separate end-rings. The magnetic circuit is fully symmetric and linearised, the air-gap between the stator and rotor is assumed to be smooth, and the field density in the air-gap has only a radial component. Under these assumptions, the equations of the circuits on the stator and rotor take a general form, given by (1).

$$\begin{bmatrix} \boldsymbol{u}^s \\ \boldsymbol{0} \\ \boldsymbol{0} \end{bmatrix} = \left(\operatorname{diag} \begin{bmatrix} \boldsymbol{R}^s \\ \boldsymbol{R}^o \\ \boldsymbol{R}^i \end{bmatrix} + \frac{\mathrm{d}}{\mathrm{d}t} \begin{bmatrix} \boldsymbol{L}^s_\sigma + L^s & \boldsymbol{L}^{sr}(\varphi) & \boldsymbol{L}^{sr}(\varphi) \\ [\boldsymbol{L}^{sr}(\varphi)]^T & \boldsymbol{L}^o_\sigma + L^o & \boldsymbol{L}^{oi} \\ [\boldsymbol{L}^{sr}(\varphi)]^T & \boldsymbol{L}^{io} & \boldsymbol{L}^i_\sigma + L^i \end{bmatrix} \right) \begin{bmatrix} \boldsymbol{i}^s \\ \boldsymbol{i}^o \\ \boldsymbol{i}^i \end{bmatrix}, \tag{1}$$

where $\boldsymbol{u}^s = [u^s_a \quad u^s_b \quad u^s_c]^T$ and $\boldsymbol{i}^s = [i^s_a \quad i^s_b \quad i^s_c]^T$ are the vectors of the stator phase voltages and currents, respectively and $\boldsymbol{i}^o = [i^o_1 \quad \ldots \quad i^o_N]^T$ and $\boldsymbol{i}^i = [i^i_1 \quad \ldots \quad i^i_N]^T$ are the vectors of the mesh currents of the outer and inner cages, respectively. Inductance matrices contain self and mutual inductances owing to the main flux: $\boldsymbol{L}^s$ of stator windings, $\boldsymbol{L}^o$ of outer cage meshes and $\boldsymbol{L}^i$ of inner cage mashes. By contrast, $\boldsymbol{L}^{sr}(\varphi)$ contains mutual inductances of stator windings to rotor meshes, both outer and inner, and $\boldsymbol{L}^{oi}$ mutual inductances between meshes of outer and inner cages. The matrices with the subscript σ contain the respective inductances owing to leakages

fluxes. Detailed forms of these matrices are not presented here because they are the same as those for classical cage motors and are well known in the literature [1, 4, 8, 9, 20]. The resistance matrices, which are essential for modelling the asymmetry of the rotor cages and stator side, are expressed as follows:

The matrix of stator phase resistance:

$$\boldsymbol{R}^s = \operatorname{diag}\left[R_a^s \quad R_b^s \quad R_c^s\right]. \tag{2}$$

Resistance matrices of the rotor cages:

$$\boldsymbol{R}^r = \begin{bmatrix} R_{m,1}^r & -R_{b,2}^r & 0 & \dots & 0 & -R_{b,1}^r \\ -R_{b,2}^r & R_{m,2}^r & -R_{b,3}^r & \dots & 0 & 0 \\ 0 & -R_{b,3}^r & R_{m,3}^r & \dots & 0 & 0 \\ \vdots & \vdots & \vdots & \ddots & \vdots & \vdots \\ 0 & 0 & 0 & & R_{m,N-1}^r & -R_{b,N}^r \\ -R_{b,1}^r & 0 & 0 & \dots & -R_{b,N}^r & R_{m,N}^r \end{bmatrix} \quad \text{for } r \in \{o, i\}. \tag{3}$$

Resistances in these matrices are given by

$$R_{m,n}^o = R_{b,n}^o + R_{b,\mathrm{mod}(n,N)+1}^o + 2R_{sc}^o \quad \text{and} \quad R_{m,n}^i = R_{b,n}^i + R_{b,\mathrm{mod}(n,N)+1}^i + 2R_{sc}^i,$$

where $R_{b,n}^o$ and $R_{b,n}^i$ are the resistances of the individual bars of the outer and inner cages, respectively, and R_{sc}^o and R_{sc}^i are the resistances of the end-ring segment between the bars in the outer and inner bars, respectively.

The spectral analysis of steady states simply identifies symmetrical components for description. Equation (1) can be written as

$$\boldsymbol{u} = \boldsymbol{R} \cdot \boldsymbol{i} + \frac{\mathrm{d}}{\mathrm{d}t}\left[\boldsymbol{L}(\varphi) \cdot \boldsymbol{i}\right].$$

Transformation to symmetrical components requires the following operaton:

$$\boldsymbol{S} \cdot \boldsymbol{u} = (\boldsymbol{S} \cdot \boldsymbol{R} \cdot \boldsymbol{S}^{-1}) \cdot (\boldsymbol{S} \cdot \boldsymbol{i}) + \frac{\mathrm{d}}{\mathrm{d}t}(\boldsymbol{S} \cdot \boldsymbol{L}(\varphi) \cdot \boldsymbol{S}^{-1}) \cdot (\boldsymbol{S} \cdot \boldsymbol{i}). \tag{4}$$

The general transformation matrix $\boldsymbol{S}$ has the form of a quasi-diagonal Hiper matrix given by

$$\boldsymbol{S} = \operatorname{diag}\left[\boldsymbol{T}_s \quad \boldsymbol{T}_r \quad \boldsymbol{T}_r\right], \tag{5}$$

where

$$\boldsymbol{T}_s = \frac{1}{\sqrt{3}}\begin{bmatrix} 1 & 1 & 1 \\ 1 & a & a^2 \\ 1 & a^2 & a \end{bmatrix}, \quad a = e^{\mathrm{j}2\pi/3}, \qquad \boldsymbol{T}_r = \frac{1}{\sqrt{N}}\begin{bmatrix} 1 & 1 & \dots & 1 \\ 1 & b & \dots & b^{N-1} \\ \vdots & \vdots & & \vdots \\ 1 & b^{N-1} & \dots & b^{(N-1)^2} \end{bmatrix}, \quad b = e^{\mathrm{j}2\pi/N}.$$

The matrix $\boldsymbol{T}_s$ defines symmetrical components of stator phase voltages and currents as

$$\boldsymbol{u}_s = \boldsymbol{T}_s \cdot \boldsymbol{u}^s = \left[u_s^0 \quad u_s^1 \quad u_s^2\right]^T, \qquad \boldsymbol{i}_s = \boldsymbol{T}_s \cdot \boldsymbol{i}^s = \left[i_s^0 \quad i_s^1 \quad i_s^2\right]^T. \tag{6}$$

By contrast, the matrix $\boldsymbol{T}_r$ defines the multiphase symmetrical components of mesh currents for both the upper and lower rotor cages, expressed as

$$\boldsymbol{i}^o = \boldsymbol{T}_r \cdot \boldsymbol{i}_o = \begin{bmatrix} i_o^0 & i_o^1 & \dots & i_o^{N-1} \end{bmatrix}^T, \qquad \boldsymbol{i}^i = \boldsymbol{T}_r \cdot \boldsymbol{i}_i = \begin{bmatrix} i_i^0 & i_i^1 & \dots & i_i^{N-1} \end{bmatrix}^T. \tag{7}$$

The resulting equations takes similar forms as that of (1).

$$\begin{bmatrix} \boldsymbol{u}_s \\ \boldsymbol{0} \\ \boldsymbol{0} \end{bmatrix} = \left(\operatorname{diag} \begin{bmatrix} \boldsymbol{R}_s \\ \boldsymbol{R}_o \\ \boldsymbol{R}_i \end{bmatrix} + \frac{\mathrm{d}}{\mathrm{d}t} \begin{bmatrix} \boldsymbol{L}_s & \boldsymbol{L}_{sr}(\varphi) & \boldsymbol{L}_{sr}(\varphi) \\ [\boldsymbol{L}_{sr}(\varphi)]^T & \boldsymbol{L}_o & \boldsymbol{L}_{oi} \\ [\boldsymbol{L}_{sr}(\varphi)]^T & [\boldsymbol{L}_{io}]^T & \boldsymbol{L}_i \end{bmatrix} \right) \begin{bmatrix} \boldsymbol{i}_s \\ \boldsymbol{i}_o \\ \boldsymbol{i}_i \end{bmatrix}. \tag{8}$$

The structures of the inductance matrices in these equations are considerably simple. In addition to the matrix $\boldsymbol{L}_{sr}(\varphi)$, all other matrices are diagonal, as shown below. Their forms are based on the matrices for a one-cage motor, as reported in the literature [4, 6, 8, 9].

$$\begin{aligned} \boldsymbol{L}_s &= \boldsymbol{L}_s^\sigma + \boldsymbol{L}_s^\mu = \operatorname{diag}\left[\boldsymbol{L}_s \quad \boldsymbol{L}_s\right] = \operatorname{diag}\left[L_s^\sigma + L_s^\mu \quad L_s^\sigma + L_s^\mu\right], \\ \boldsymbol{L}_r &= \operatorname{diag}\left[L_{o,r}^0 \quad L_{o,r}^1 + L_r^\mu \quad \dots \quad L_{\sigma,r}^{N-1} + L_r^\mu\right], \quad \text{for } r \in \{oi\}, \\ \boldsymbol{L}_{oi} &= \operatorname{diag}\left[0 \quad L_r^\mu \quad \dots \quad L_r^\mu\right]. \end{aligned}$$

The matrix $\boldsymbol{L}_{sr}(\varphi)$ has a very specific form. Its Fourier series contains only odd harmonics with respect to the pole-pair number p owing to the assumed symmetry of the stator winding. The matrix is expressed as

$$\boldsymbol{L}_{sr}(\varphi) = \sum_{m=-\infty}^{\infty} \boldsymbol{L}_{sr,m} \cdot e^{\mathrm{j}m\varphi}, \quad \text{for } m \in \{\pm p, \pm 3p, \pm 5p, \dots\}.$$

The coefficients of this matrix Fourier series, the matrices $\boldsymbol{L}_{sr,m}$ with dimensions, have only one non-zero element in the column $\operatorname{mod}(mp, N-1)$ and row $\operatorname{mod}(m, 3)$.

The resistance matrices, which are important for analysing the asymmetry in a double rotor, are determined using the following relations:

$$\boldsymbol{R}_s = \boldsymbol{T}_s \cdot \boldsymbol{R}^s \cdot \boldsymbol{T}_s^{-1}, \qquad \boldsymbol{R}_o = \boldsymbol{T}_r \cdot \boldsymbol{R}^o \cdot \boldsymbol{T}_r^{-1}, \qquad \boldsymbol{R}_i = \boldsymbol{T}_r \cdot \boldsymbol{R}^i \cdot \boldsymbol{T}_r^{-1}. \tag{9}$$

The respective resistance matrices of rotor cages become full if asymmetry arises. Furthermore, by studying the double cage asymmetry, Equation set (8) has a dimension of $(3 + 2N)$, which is large for rotors with many slots.

Equations (8) is useful for direct spectral analysis at steady state operations, particularly at a constant rotor angular velocity; that is, during $\varphi = \Omega \cdot t + \varphi_0$. The matrix $\boldsymbol{L}_{sr}(\varphi)$ for such conditions becomes periodic and can be extended to a Fourier series, expressed as

$$\boldsymbol{L}_{sr}(\varphi) = \boldsymbol{L}_{sr}(t) = \boldsymbol{L}_{sr}(t+T) = \sum_{m=-\infty}^{\infty} L_{sr,m} \cdot e^{\mathrm{j}mp\Omega t}, \tag{10}$$

where only odd harmonics with respect to the pole-pair number occur; that is, for $m \in \{\pm 1, \pm 3, \dots\}$, owing to the assumed symmetry of the stator winding. The Fourier spectra of all currents can be determined by balancing harmonics of voltages, inductances, and currents using the harmonic balance method [2, 3, 8–10, 14, 20].

3. Harmonic balance equations

Harmonic balance equations are presented as steady states at an arbitrary constant angular velocity Ω = const for monoharmonic, symmetrical stator phase voltages with pulsation Ω_s, assuming star connection of stator phases without neutral. The star connection without neutral eliminates the equation for zero components of stator values; therefore, in Eq. (8) vectors of voltage $\boldsymbol{u}_s$ and current $\boldsymbol{i}_s$ can be reduced to

$$\boldsymbol{u}_s = \begin{bmatrix} u_s^1 & \overset{*}{u}{}_s^1 \end{bmatrix}^T, \qquad \boldsymbol{i}_s = \begin{bmatrix} i_s^1 & \overset{*}{i}{}_s^1 \end{bmatrix}^T, \tag{11}$$

where $u_s^1 = \sqrt{3}U \cdot e^{\mathrm{j}\Omega_s t}$ and are the RMS values of the phase voltages. Consequently, it is sufficient to obtain the harmonic balance equations for forced vector $\boldsymbol{u}_s^1 = \begin{bmatrix} u_s^1 & 0 \end{bmatrix}^T$. Under these conditions, the vector of the currents in the steady state can be predicted using the following Fourier series:

$$\boldsymbol{i}_s^1 = \begin{bmatrix} i_s^{1,1} & i_s^{1,2} \end{bmatrix}^T = \sum_{m=-\infty}^{\infty} \begin{bmatrix} I_{s,m}^1 & I_{s,m}^2 \end{bmatrix}^T e^{\mathrm{j}(\Omega_s + pm\Omega)\cdot t}, \tag{12}$$

$$\begin{aligned} \boldsymbol{i}_r^1 &= \begin{bmatrix} i_r^{1,0} & i_r^{1,1} & \dots & i_r^{1,N-1} \end{bmatrix}^T \\ &= \sum_{m=-\infty}^{\infty} [I_{r,m}^{1,0} e^{\mathrm{j}pm\varphi_0} \quad \dots \quad I_{r,m}^{1,N-1} e^{\mathrm{j}pm\varphi_0}]^T e^{\mathrm{j}(\Omega_s + pm\Omega)t}, \quad \text{for } r \in \{o,i\}. \end{aligned} \tag{13}$$

Harmonic balance equations formulate the relations between the coefficients of all Fourier series for voltages, resistances, inductances, and currents. The following form is considered for the steady states

$$\begin{bmatrix} \boldsymbol{u}_s \\ \boldsymbol{0} \\ \boldsymbol{0} \end{bmatrix} = \left(\operatorname{diag} \begin{bmatrix} \boldsymbol{R}_s \\ \boldsymbol{R}_o \\ \boldsymbol{R}_i \end{bmatrix} + \mathrm{j} \cdot \operatorname{diag} \begin{bmatrix} \boldsymbol{\Omega}_s \\ \boldsymbol{\Omega}_r \\ \boldsymbol{\Omega}_r \end{bmatrix} \cdot \begin{bmatrix} \boldsymbol{L}_s & \boldsymbol{L}_{sr} & \boldsymbol{L}_{sr} \\ \overset{*}{[\boldsymbol{L}_{sr}]}{}^T & \boldsymbol{L}_o & \boldsymbol{L}_{oi} \\ \overset{*}{[\boldsymbol{L}_{sr}]}{}^T & \boldsymbol{L}_{io} & \boldsymbol{L}_i \end{bmatrix} \right) \begin{bmatrix} \boldsymbol{i}_s \\ \boldsymbol{i}_o \\ \boldsymbol{i}_i \end{bmatrix}. \tag{14}$$

These equations constitute an infinite set of algebraic equations, with complex variables and parameters. The arrangement of vectors representing the voltages and currents is shown below.

The only non-zero forced vector $\boldsymbol{u}_s$ on the left-hand side, arranged with respect to the central element representing the u_s^1 voltage, takes the form

$$\boldsymbol{u}_s = \begin{bmatrix} \boldsymbol{u}_s^1 & \boldsymbol{u}_s^2 \end{bmatrix}^T, \qquad \boldsymbol{u}_s^1 = [\dots \quad 0 \quad \sqrt{3}U \quad 0 \quad \dots]^T, \qquad \boldsymbol{u}_s^2 = [\dots \quad 0 \quad 0 \quad 0 \quad \dots]^T. \tag{15}$$

The arrangement of the current vector $\boldsymbol{i}_s$ follows that of the vector $\boldsymbol{u}_s$.

$$\begin{aligned} \boldsymbol{i}_s &= \begin{bmatrix} \boldsymbol{i}_s^1 & \boldsymbol{i}_s^2 \end{bmatrix}^T, \qquad \boldsymbol{i}_s^1 = \begin{bmatrix} \dots & I_{s,1}^1 & I_{s,0}^1 & I_{s,-1}^1 & \dots \end{bmatrix}^T, \\ \boldsymbol{i}_s^2 &= \begin{bmatrix} \dots & I_{s,1}^2 & I_{s,0}^2 & I_{s,-1}^2 & \dots \end{bmatrix}^T. \end{aligned} \tag{16}$$

The vectors of the cage currents are expressed as

$$\boldsymbol{i}_r = \begin{bmatrix} \dots & I_{r,1}^1 & I_{r,0}^1 & I_{r,-1}^1 & \dots \end{bmatrix}^T, \quad \text{where} \quad \boldsymbol{I}_{r,m}^{1,0} = \begin{bmatrix} I_{r,m}^{1,0} & \dots & I_{r,m}^{1,N-1} \end{bmatrix}^T, \text{ for } r \in \{o,i\}. \tag{17}$$

The second terms in the lower subscripts in (16) and (17) follows the subscript m in the Fourier series (12) and (13).

The asymmetry of rotor cages and the break of one from stator phases is modelled by the matrices $\boldsymbol{R}_s$, $\boldsymbol{R}_o$ and $\boldsymbol{R}_i$ in (8), which are full but with constant elements. The matrices $\boldsymbol{R}_s$, $\boldsymbol{R}_o$ and $\boldsymbol{R}_i$ in (14) contain these matrices. The matrix $\boldsymbol{R}_s$, for the arrangements of stator currents as in (16) takes the following form:

$$\boldsymbol{R}_s = \begin{bmatrix} \boldsymbol{R}_s^0 & \boldsymbol{R}_s^2 \\ \overset{*}{\boldsymbol{R}}_s^2 & \boldsymbol{R}_s^0 \end{bmatrix}.$$

The infinite matrices $\boldsymbol{R}_s^0$ and $\boldsymbol{R}_s^2$, as shown below, are diagonal.

$$\boldsymbol{R}_s^0 = \operatorname{diag}\left[\ldots \quad R_s^0 \quad R_s^0 \quad R_s^0 \quad \ldots\right], \qquad \boldsymbol{R}_s^2 = \operatorname{diag}\left[\ldots \quad \underline{R}_s^2 \quad \underline{R}_s^2 \quad \underline{R}_s^2 \quad \ldots\right]$$

with elements

$$R_s^0 = \frac{1}{3} \cdot \left(R_a^s + R_b^s + R_c^s\right) \quad \text{and} \quad R_s^2 = \frac{1}{3} \cdot \left(R_a^s + a^2 R_b^s + a R_c^s\right).$$

The infinite matrices $\boldsymbol{R}_o$ and $\boldsymbol{R}_i$ are quasi-diagonal with the respective matrices $\boldsymbol{R}_o$ and $\boldsymbol{R}_i$ on the main diagonal.

The symmetry of the magnetic circuit and stator winding, assumed for the mathematical model, causes all inductance matrices in (14), in addition to $\boldsymbol{L}_{sr}$, to be diagonal with constant elements. The matrix has the form:

$$\boldsymbol{L}_s = \operatorname{diag}\left[L_s^1 \quad L_s^2\right], \quad \text{where} \quad \boldsymbol{L}_s^1 = \boldsymbol{L}_s^1 = \operatorname{diag}\left[\ldots \quad L_s \quad L_s \quad L_s \quad \ldots\right].$$

The infinite matrices $\boldsymbol{L}_o$, $\boldsymbol{L}_i$, and $\boldsymbol{L}_{oi}$ are quasi-diagonal with the matrices $\boldsymbol{L}_o$, $\boldsymbol{L}_i$, and $\boldsymbol{L}_{oi}$ on the primary diagonal, respectively. The structure of the matrix $\boldsymbol{L}_{sr}$ is most important for modelling harmonic interactions. The transpose of the matrix is created by two infinite matrices $\boldsymbol{L}_{sr} = \left[\boldsymbol{L}_{sr}^1 \quad \boldsymbol{L}_{sr}^2\right]^T$ with the following structures:

$$\boldsymbol{L}_{sr}^1 = \begin{bmatrix}
\ddots & \ddots & \ddots & \ddots & \ddots & \ddots & \ddots & \ddots & \\
\ddots & \mathbf{0} & \ldots & L_p & \mathbf{0} & \ldots & L_{7p} & \mathbf{0} & \ddots \\
\ddots & \ldots & \mathbf{0} & \ldots & L_p & \mathbf{0} & \ldots & L_{7p} & \ddots \\
\ddots & L_{-5p} & \ldots & \mathbf{0} & \ldots & L_p & \mathbf{0} & \ldots & \ddots \\
\ddots & \mathbf{0} & L_{-5p} & \ldots & \mathbf{0} & \ldots & L_p & \mathbf{0} & \ddots \\
\ddots & \ldots & \mathbf{0} & L_{-5p} & \ldots & \mathbf{0} & \ldots & L_p & \ddots \\
\ddots & L_{-11p} & \ldots & \mathbf{0} & L_{-5p} & \ldots & \mathbf{0} & \ldots & \ddots \\
\ddots & \mathbf{0} & L_{-11p} & \ldots & \mathbf{0} & L_{-5p} & \ldots & \mathbf{0} & \ddots \\
 & \ddots & \ddots & \ddots & \ddots & \ddots & \ddots & \ddots & \ddots
\end{bmatrix},$$

$$\boldsymbol{L}_{sr}^{2} = \begin{bmatrix} \ddots & \ddots & \ddots & \ddots & \ddots & \ddots & \ddots & \ddots & \\ \ddots & \mathbf{0} & \dots & L_{5p} & \mathbf{0} & \dots & L_{11p} & \mathbf{0} & \ddots \\ \ddots & \dots & \mathbf{0} & \dots & L_{5p} & \mathbf{0} & \dots & L_{11p} & \ddots \\ \ddots & L_{-p} & \dots & \mathbf{0} & \dots & L_{5p} & \mathbf{0} & \dots & \ddots \\ \ddots & \mathbf{0} & L_{-p} & \dots & \mathbf{0} & \dots & L_{5p} & \mathbf{0} & \ddots \\ \ddots & \dots & \mathbf{0} & L_{-p} & \dots & \mathbf{0} & \dots & L_{5p} & \ddots \\ \ddots & L_{-7p} & \dots & \mathbf{0} & L_{-p} & \dots & \mathbf{0} & \dots & \ddots \\ \ddots & \mathbf{0} & L_{-7p} & \dots & \mathbf{0} & L_{-p} & \dots & \mathbf{0} & \ddots \\ & \ddots & \ddots & \ddots & \ddots & \ddots & \ddots & \ddots & \ddots \end{bmatrix}.$$

The inside matrices have a dimension of $(3 \times N)$. Each matrix has only one non-zero element $\underline{L}_{mp} = L_{mp} \cdot e^{\mathrm{j} \times mp\varphi_0}$ in the column mod $(mp, N-1)$ with respect to the harmonic order.

Differentiation operators in frequency domain have a diagonal structure, expressed as

$$\begin{aligned} \boldsymbol{\Omega}_o &= \operatorname{diag}\left[\boldsymbol{\Omega}_s \quad \boldsymbol{\Omega}_s\right], \\ \boldsymbol{\Omega}_s &= \operatorname{diag}\left[\dots \quad (\Omega_s + p\Omega) \quad \boldsymbol{\Omega}_s \quad (\Omega_s - p\Omega) \quad \dots\right], \\ \boldsymbol{\Omega}_r &= \operatorname{diag}\left[\dots \quad (\Omega_s + p\Omega)\boldsymbol{E} \quad \Omega_s\boldsymbol{E} \quad (\Omega_s - p\Omega)\boldsymbol{E} \quad \dots\right]. \end{aligned}$$

A detailed analysis of Eq. (14) quantitatively determines the stator current Fourier spectra. The results of this analysis indicates that at any fault in the rotor cages, outer and inner, a symmetrical supply is generated in the stator component $i_s^{1,1}$ (defined in (12)), harmonics with pulsations $\Omega_s + 6kp\Omega$, and component $i_s^{1,2}$ harmonics with pulsations $\Omega_s - (2+6k)p\Omega$, for $k \in \{\pm 1, \pm 2, \dots\}$. The spectra change qualitatively when one stator phase is broken at the same fault in the rotor. The stator current components and contain harmonics with pulsations $\Omega_s + 2kp\Omega$. Table 1 summarises the results. The harmonics observed in the stator phase current spectra have a frequency of $f_h = 2\pi / \|\Omega_h\|$.

Table 1. Qualitative features of stator current spectra

Type of asymmetry	**Stator currents component**	**Pulsations**
Faults in cages, symmetrical supply	$i_s^{1,1}$	$\Omega_s + 6kp\Omega$
	$i_s^{1,2}$	$\Omega_s - (2+6k)p\Omega$
Faults in cages, one-phase supply	$i_s^{1,1}$	$\Omega_s + 2kp\Omega$
	$i_s^{1,2}$	$\Omega_s + 2kp\Omega$

$k \in \{\pm 1, \pm 2, \dots\}$.

With a symmetrical supply and small slip, the inner cage is more active, and faults in the inner cage should be more apparent. The abovementioned tests could indicate faults in the inner cage. With one-phase supply, the backward MMF is generated by stator phases, activating the

outer cage. Therefore, faults in this cage should be apparent, and the test can indicate faults in the outer cage. These suggestions were confirmed by the results of the numerical tests presented in the next chapter.

4. Results of numerical tests

The numerical calculations were performed to quantitatively confirm if the abovementioned tests can distinguish between faults in the upper and lower cages. Accordingly, harmonic Eqs. (14) were solved. The equations are infinitive. The calculations were limited to a finite number, considering the matrix $\boldsymbol{L}_{sr}$ harmonics up to $17p$. These limited equations contain the Fourier coefficients of currents with frequencies up to 1.5 kHz. A set of 8 199 algebraic complex equations were solved after structural analysis of (14). A MATLAB code was prepared using an iterative procedure for the sparse matrices. The equation parameters were determined using the geometrical and material data of the magnetic circuit, stator winding, and rotor cages.

Two tests were provided, described as follows:

Test 1

The stator current spectra with symmetrical supply were calculated for the near-rated load. Three faults were assumed to be representative.

– One broken bar in the outer cage,
– One broken bar in the inner cage in the same slot,
– Two broken bars: one in outer and one in inner cages in the same slot.

Test 2

The stator current spectra with one-phase supply were calculated for an almost idle running motor. The type of rotor fault was the same as that in Test 1.

– One broken bar in the outer cage,
– One broken bar in the inner cage in the same slot,
– Two broken bars: one in outer and one in inner cages in the same slot.

Calculations were performed for a motor with rated data: $P_N = 160$ kW, $U_N = 1.0$ kV, $I_N = 114$ A, and $n_N = 1\,485$ rpm, connected in star without neutral. Table 2 presents the geometric and design data. Table 3 presents the parameters of the rotor bars in the outer and inner cages. The damage to the rotor bars was modelled by growing its resistance by 20 times. The braking of the stator phase was simulated by increasing the phase resistance to 10^6 Ω.

Table 2. Geometrical and design data

Parameter name	Symbol	Value	Unit
Yoke axial length	L_{Fe}	0.31	m
Air gap thickness	δ	0.0025	m
Stator inner diameter	d_s	0.16	m
Number of stator/rotor slots	N_s/N_r	48/38	–
Average stator winding pitch	Y	11	–
Number of turns per phase	Z_s	168	–

Table 3. Parameters of rotor cages

Parameter name	Symbol	Value	Unit
Upper/lower cage bar resistance	R_b^o/R_b^i	0.42/0.05	mΩ
Upper/lower cage bar inductance	L_b^o/L_b^i	0.7/2.5	μH
Upper/lower cage segment res.	R_{sc}^o/R_{sc}^i	1.1/0.6	μΩ
Upper/lower cage segment res.	L_{sc}^o/L_{sc}^i	0.03/0.025	μH

Figures 1(a), (b), and (c) show the results of Test 1. The Fourier spectra of the stator current symmetrical components $i_s^{1,1}$ and $i_s^{1,2}$ versus pulsations for all three faults are shown with a 10^{-5} A reference level.

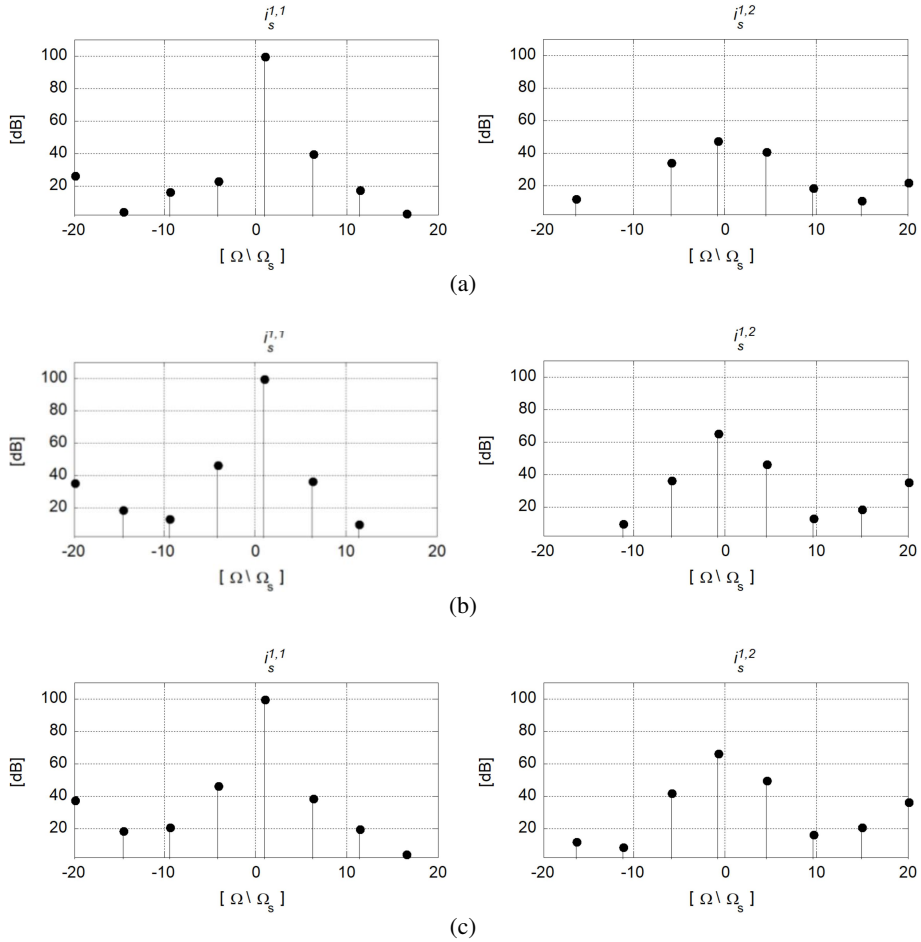

Fig. 1. Spectra of stator current symmetrical components $i_s^{1,1}$ and $i_s^{1,12}$ with a symmetrical supply and faults in rotor cages: (a) one broken bar in outer cage; (b) one broken bar in inner cage; (c) broken bars in the same slot in upper and inner cages

The harmonics in these spectra have pulsations, as listed in Table 3. Individual components maintain the distance $6p\Omega$, symmetrically with respect to the basic component with pulsation Ω_s for the current $i_s^{1,1}$ and with respect to the component with pulsation $-p\Omega$ for the current $i_s^{1,2}$. Figures 2(a), (b) and (c) show the Fourier spectra of the stator phase current versus frequency up to 1 kHz.

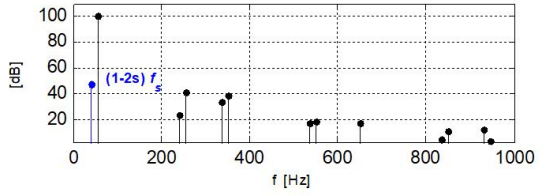

(a)

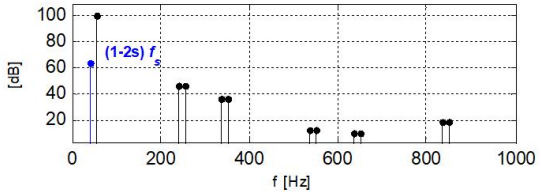

(b)

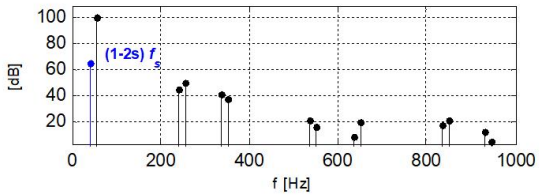

(c)

Fig. 2. Spectra of a stator phase current with a symmetrical supply and faults in rotor cages: (a) one broken bar in outer cage; (b) one broken bar in inner cage; (c) broken bars in the same slot in upper and inner cages

From a diagnostic point of view, the most promising component is frequency $(1-2s)f_s$ with frequency (s is a rotor slip), which is characteristic of cage asymmetry. This component is 20 dB greater when one bar is broken in the inner cage (i.e., working cage) than when one bar is broken in the outer (starting) cage, with the same supply under load conditions. Therefore, the appearance of the component with frequency at normal steady state operation indicates a fault in the inner cage. The spectra presented in Fig. 1 do not contain components typically observed with frequency $(1+2s)f_s$. This is because of a constant rotor speed assumed for the spectral analysis of currents. However, this component is strictly related to component $(1-2s)f_s$ depends on the moment of inertia of the drive, and can be neglected or summed with that first.

Figures 3(a), (b), and (c) show the results of Test 2. The Fourier spectra of the stator current symmetrical components $i_s^{1,1}$ and $i_s^{1,2}$ versus the pulsations for all three faults are shown with a 10^{-5} A reference level.

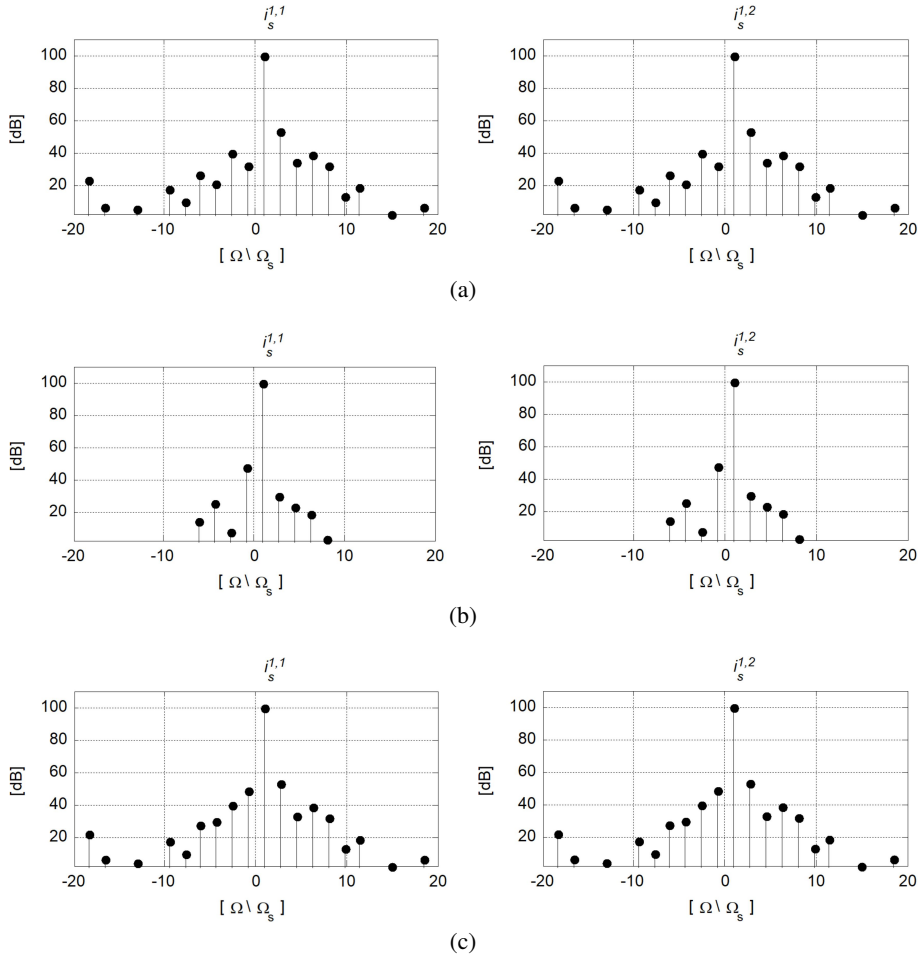

Fig. 3. Spectra of stator current symmetrical components $i_s^{1,1}$ and $i_s^{1,2}$ at one broken phase and faults in rotor cages: (a) one broken bar in outer cage; (b) one broken bar in inner cage; (c) broken bars in the same slot in upper and inner cages

The harmonics in these spectra have pulsations, as listed in Table 3. The spectra qualitatively have the same harmonics for the symmetrical components of $i_s^{1,1}$ and $i_s^{1,2}$. Individual components maintain a distance of $2p\Omega$ with respect to Ω_s, both for currents $i_s^{1,1}$ and $i_s^{1,2}$.

Figures 4(a), (b), and (c) show the Fourier spectra of the stator phase current versus frequency up to 1 kHz. The asymmetry on the stator side generates new components in the stator current, as shown in Fig. 4. Moreover, diagnostic components with frequencies near $3f_s$, (i.e., $(3-2s)f_s$ and

$(3-4s)f_s$), are the greater number of new components when a fault in the outer cage appears. Stotor asymmetry generates the backward component of the rotating magnetic field in a motor, activating the outer cage. Its asymmetry is much more apparent in the stator current spectrum than that of faults in the inner cage. The spectra in Figs. 4(a), (b), and (c) confirm these findings. Therefore, the appearance of the components with frequencies near in the stator current spectrum with the broken one phase and non-load state indicates a fault in the outer cage.

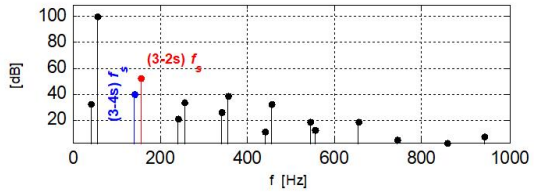

(a)

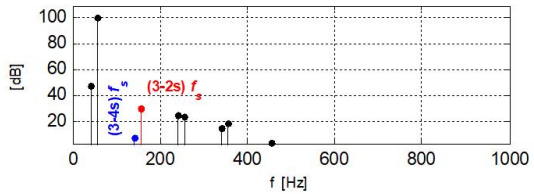

(b)

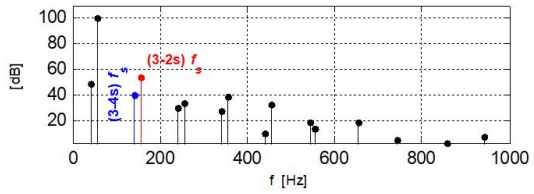

(c)

Fig. 4. Spectra of a stator phase current with one-phase supply and faults in rotor cages: (a) one broken bar in outer cage; (b) one broken bar in inner cage; (c) broken bars in the same slot in upper cage and inner cages

These two tests show and explain the basic effects which can be applied to the diagnosis of double-cage rotors using motor current signature analysis.

5. Conclusions

This study presents the stator phase current spectral analysis method for double-cage induction motors to diagnose faults in rotor cages. It is based on a mathematical model that considers the details of the rotor design used to describe the symmetrical components of the stator and rotor values. Spectral analysis was performed using the harmonic balance method to algebraize the

problem. Two tests were proposed, which suggested diagnostic signals based on the stator current spectra at steady states for normal operation and at one broken stator phase for the idle run. Numerical tests quantitatively confirmed the possibility of distinguishing between faults in the outer (starting) and inner (working) cages.

The stator current spectra, obtained from the approach presented in this study, can be a basis for more advanced motor current signature analysis often applied to diagnose induction motors. Moreover, the spectra can create a data basis for diagnostics using artificial intelligence algorithms.

References

[1] Taegen F., Hommes E., *Das allgemeine Gleichungssystem des Käfigläufermotors unter Berücksichtigung der Oberfelder*, Teil I: Allgemeine Theorie, Archiv für Elektrotechnik, Springer-Verlag, vol. 52, pp. 21–31 (1972), DOI: 10.1007/BF01407854.

[2] Sobczyk T., *Infinitely dimensional linear and quadratic forms of electric machines*, Rozprawy Elektrotechniczne, PWN, vol. 29, bull. 1, pp. 697–707 (1983).

[3] Sobczyk T., *Equations of Squirrel-Cage Induction Motors with Symmetrical Design in Steady-State Operation*, Rozprawy Elektrotechniczne, PWN, vol. 33, bull. 1, pp. 137–149 (1987).

[4] Drozdowski P., Sobczyk T.J., *On a mathematical model of squirrel-cage induction motor*, Archiv fur Elektrotechnik, Springer-Verlag, vol. 70, pp. 371–382 (1987), DOI: 10.1007/BF01574005.

[5] Williamson S., Abdel-Magied M.A.S., *Steady-state analysis of double-cage induction motors with rotor-cage faults*, IEE Proceedings B (Electric Power Applications), vol. 134, no. 4, pp. 199–206 (1987), DOI: 10.1049/ip-b.1987.0034.

[6] Sobczyk T.J., Weinreb K., *Analysis of currents and an electromagnetic torque in steady states of induction squirrel-cage motors with asymmetric stator windings*, Archiv für Elektrotechnik, Springer-Verlag, vol. 71, pp. 245–256 (1988), DOI: 10.1007/BF01580174.

[7] Nabeta S.I., Chabu I.E., Cardoso J.R., Foggia A., *Double-cage induction motor modelling using finite elements*, Electric Machines and Drives Conference, Milwaukee, WI, USA, pp. 1–3 (1997), DOI: 10.1109/IEMDC.1997.604291.

[8] Rusek J., *Categorization of induction machines in current signature analysis*, Electrical Engineering, Springer-Verlag, vol. 84, pp. 265–273 (2002), DOI: 10.1007/s00202-002-0131-9.

[9] Sobczyk T.J., *Methodical aspects of mathematical modeling of induction machines*, WNT (in Polish), Warsaw (2004).

[10] Sobczyk T.J., *Frequency analysis of faulty machines – possibilities and limitations*, IEEE Int. Symp. on Diagnostics for Electric Machines, Power Electronics and Drives, Cracow, Poland, pp. 1–5 (2007), DOI: 10.1109/DEMPED.2007.4393081.

[11] Pitis C.D., *Thermo-mechanical stresses of the squirrel cage rotors in adverse load conditions*, Int. Symp. Electrical Insulation, Vancouver, BC, Canada, pp. 1–7 (2008), DOI: 10.1109/ELINSL.2008.4570399.

[12] Boldea I., Nasad Syed A., *The Induction Machines Design Handbook*, 2^{nd} Edition, CRC Press (2009), DOI: 10.1201/9781315222592.

[13] Park J., Kim B., Lee K., Lee S.B., Wiedenbrug E.J., Teska M., Han S., *Evaluation of the detectability of broken rotor bars for double squirrel cage rotor induction motors*, IEEE Energy Conversion Congress and Exposition, Atlanta, GA, USA, pp. 2493–2500 (2010), DOI: 10.1109/ECCE.2010.5617950.

[14] Węgiel T., Weinreb K., Sułowicz M., *Main inductances of induction motor for diagnostically specialized mathematical models*, Archives of Electrical Engineering, vol. 59, no. 1–2, pp. 51–66 (2010), DOI: 10.2478/s10171-010-0004-1.

[15] Antonino-Daviu J., Riera-Guasp M., Pons-Llinares J., Park J., Lee S.B., Yoo J., Kral C., *Detection of broken outer-cage bars for double-cage induction motors under the startup transient*, IEEE Transactions on Industry Applications, vol. 5, no. 48, pp. 1539–1548 (2012), DOI: 10.1109/TIA.2012.2210173.

[16] Gritli Y., Di Tommaso A.O., Filippetti F., Miceli R., Rossi C., Chatti A., *Investigation of motor current signature and vibration analysis for diagnosing rotor broken bars in double cage in-duction motors*, Int. Symp. on Power Electronics, Electrical Drives, Automation and Motion, Sorrento, Italy, pp. 1360–1365 (2012), DOI: 10.1109/SPEEDAM.2012.6264465.

[17] Gritli Y., Di Tommaso A.O., Filippetti F., Miceli R., Rossi C., *Vibration signature analysis for rotor broken bar diagnosis in double cage induction motor drives*, 4^{th} International Conference on Power Engineering, Energy and Electrical Drives, Istanbul, Turkey, pp. 1814–1820 (2013), DOI: 10.1109/PowerEng.2013.6635893.

[18] Gyftakis K.N., Athanasopoulos D.K., Kappatou J., *Broken bar fault diagnosis in single and double cage induction motors fed by asymmetrical voltage supply*, IEEE Int. Symp. on Diagnostics for Electric Machines, Power Electronics and Drives, Valencia, Spain, pp. 402–406 (2013), DOI: 10.1109/DEMPED.2013.6645747.

[19] Pyrhonen J., Jokinen T., Hrabovcova V., *Design of rotating electrical machines*, 2nd Edition, John Wiley & Sons (2013), DOI: 10.1002/9781118701591.

[20] Weinreb K., *Diagnostics of an induction-motor rotor by the spectral analysis of stator currents*, Thermal Engineering, Springer US, vol. 60, no. 14, pp. 1006–1023 (2013), DOI: 10.1134/S0040601513140073.

[21] Gritli Y., Lee S.B., Filippetti F., Zarri L., *Advanced diagnosis of outer cage damage in double-squirrel-cage induction motors under time-varying conditions based on wavelet analysis*, IEEE Transactions on Industry Applications, vol. 3, no. 50, pp. 1791–1800 (2014), DOI: 10.1109/TIA.2013.2285958.

[22] Pons-Llinares J., Antonino-Daviu J., Riera-Guasp M., Lee S.B., Kang T.-J., Yang C., *Advanced induction motor rotor fault diagnosis via continuous and discrete time–frequency tools*, IEEE Transactions on Industrial Electronics, vol. 62, no. 3, pp. 1791–1802 (2015), DOI: 10.1109/TIE.2014.2355816.

[23] Mróz J., *The model of double-cage induction motor for the analysis of thermal fields in transient operations*, Archives of Electrical Engineering, vol. 66, no. 2, pp. 397–408 (2017), DOI: 10.1515/aee-2017-0030.

[24] Tulicki J., Weinreb K., Sułowicz M., *The possibility of distinguishing rotor cage bar faults in double squirrel cage induction motors on the basis of the stator current signal*, Int. Symp. on Electrical Machines (SME), Naleczow, Poland, pp. 1–6 (2017), DOI: 10.1109/ISEM.2017.7993563.

[25] Hmida M.A., Braham A., *An on-line condition monitoring system for incipient fault detection in double-cage induction motor*, IEEE Transactions on Instrumentation and Measurement, vol. 67, no. 8, pp. 1850–1858 (2018), DOI: 10.1109/TIM.2018.2806009.

[26] Kim D.H., Choi J.H., Kim K.S., Lee J., Kim W.H., *Design process of working bar of double-cage induction motor*, IEEE Transactions on Applied Superconductivity, vol. 30, no. 4, pp. 1–5 (2020), DOI: 10.1109/TASC.2020.2976965.

[27] Kim D.H., Kim K.S., Lee J., Yang I.J., Song S.W., Kim W.H., *Study on performance improvement by rotating working bar of double-cage induction motor*, IEEE Energy Conversion Congress and Exposition (ECCE), Detroit, MI, USA, pp. 2042–2045 (2020), DOI: 10.1109/ECCE44975.2020.9236269.

[28] Bouabid N., Moussa M.A., Maouche Y., Khezzar A., *The effect of closed loop control on diagnostic indices in different faults of squirrel cage induction motor*, Archives of Electrical Engineering, vol. 70, no. 4, pp. 943–958 (2021), DOI: 10.24425/aee.2021.138271.